Cement and Concrete Research 39 (2009) 401–408

Contents lists available at ScienceDirect

Cement and Concrete Research

journal homepage: http://ees.elsevier.com/CEMCON/default.asp

Yield stress during setting of cement pastes from penetration tests

D. Lootens [a,*], P. Jousset [a], L. Martinie [b], N. Roussel [b], R.J. Flatt [a]

[a] Sika Technology AG, CH-8048 Zurich, Switzerland
[b] Université Paris Est, Laboratoire Central des Ponts et Chaussées, Paris 75732 Cedex 15, France

ARTICLE INFO

Article history:
Received 18 March 2008
Accepted 29 January 2009

Keywords:
Rheology
Yield stress
Penetration tests

ABSTRACT

Measurements of highly visco-elastic media such as cementitious materials during hardening and setting are difficult with standard rheometers. That is why the transition between liquid and solid state of cement based materials is currently measured with standardized penetration tools such as Vicat needles, ball indentation, penetrometers and Hilti nail guns. The obtained results however depend on the measuring device and only give information in arbitrary units. Moreover, no existing theory correlates these tests together although empirical correlations between the Vicat, the Proctor or the Hilti nail gun measurements and more classical rheology can be found in literature. In the present paper, an overview of this type of test is presented. By examining in detail experimental results, elasto-plastic finite elements simulations and visco-plastic fluid dynamic simulations in the specific case of penetrometer test, it is demonstrated that there exists a systematic correlation between these test results and the yield stress of the tested material. Finally more general analytical relations for several penetration tests between yield stress of the tested material and experimental data are proposed.

1. Introduction

Various empirical tests are used to study the hardening and setting of cementitious materials. These are sometimes alternatively described as consistency or setting time measurements. They include the Vicat needle, penetrometers of various shapes and the proctometer also known as the Proctor needle, as well as the Hilti nail gun. Some of these techniques measure the penetration resistance under an imposed speed, while others measure the penetration depth for an imposed load. They however all study the capacity of the tested material to prevent the penetration of a given tool. Their execution is typically carried out following a series of standardized procedures as summarized in Table 1.

Although these techniques are widely used, there is only scarce literature dealing with the correlation of the test results with any physical or mechanical properties of the material. Consequently, there are also few studies convincingly showing how to relate these tests among each other.

The main reason for this probably lies in the fact that, up to recently, it was not possible to follow the evolution of a quantifiable physical or mechanical property of cement paste during setting. Consequently, these penetration tests have remained empirical, delivering strictly comparative values. The recent development of ultrasound spectroscopy allows for the measurement of the evolutions of both shear and bulk modulus during the setting of cement paste. Based on this new technique, Lootens et al [1] demonstrated the existence of a relation between shear yield stress and the force measured by penetrometers. In that paper and the following one [2], finite element simulations supported the correlations obtained from a simple dimensional approach. The present paper expands this work to other geometries and adds to the above comparison some recent results obtained from computational fluid dynamics tools, which allow for a better understanding of the underlying mechanics. Moreover, some analytical relations between the result of the test and the yield stress of the tested material are built and validated for various tools amongst the penetration tests family.

2. Penetration tests

Several types of penetration tests exist in the field of civil engineering. Among these tests, the following ones are the most used.

2.1. Vicat needle

The Vicat needle test consists in letting a loaded needle (300 g, 1 mm in diameter) penetrate a hydrating sample and measuring the depth of penetration. Repeated tests can be performed at different positions until the sample is too hard for the needle to penetrate it. The start and end of setting are defined by standard penetration depths which are 25 mm for the Vicat initial time of setting and 0 mm for the final time of setting. These values are arbitrary and can only be used on a comparative basis. They are however not appropriate for concrete because of the large aggregates [3,4]. In terms of setting time, the use of normalized

* Corresponding author.

0008-8846/$ – see front matter © 2009 Elsevier Ltd. All rights reserved.
doi:10.1016/j.cemconres.2009.01.012

Table 1
Characteristics of penetration tests.

Test	Measurement type	Remarks	Norm
Vicat	Measurement of penetration depth for an imposed load.	Not continuous, but multiple measurements at different points (possibly automated).	C 191 C 807-99
Penetrometer	Measurement of a force to maintain a given speed.	Continuous at the same location (automated).	D 3441-79 D 1558-84
Proctor needle	Measurement of the force needed for the needle to reach a depth of 25 mm.	Not continuous, but multiple measurements at different points (manual).	C403 C1117/89
Hilti needle	Measurement of the depth reached by a nail shot.	Not continuous, but multiple measurements at different points (manual).	EN 14488-2

penetration depth is equivalent to fixing a value of the consistency of the material. It is therefore clearly a mechanical definition of setting and the link to hydration degree is therefore only indirect.

2.2. Penetrometers

Penetrometers are instruments that support a sample into which they drive a needle at a given speed and measure the force required to do so over time. An important aspect is that the needle tip is wider than the rod on which it is mounted as represented in Fig. 1. Consequently, samples with yield stress above a minimum value (not defined here) do not close up the gap above the tip and the load bearing surface S is constant during the experiment and then independent of the penetration depth. If the penetration speed is low, a measured change in force over time during penetration can therefore be attributed not to the deeper penetration of the needle but to a change of the material rheological behavior. Results tend to be reported after dividing the applied load in Newton by a calibration constant to give pressures in MPa. Using this convention, the initial and final setting times are determined when the stress reaches 3.5 MPa and 27.6 MPa respectively. The penetrometer operates at a very slow speed (1 μm/s), making the measurement quasi-static, which simplifies analysis. In comparison, measurements done with the Proctometer described below are carried out at a much higher velocity. As in the case of the Vicat needles, this definition of setting is linked to mechanical properties and not to the degree of hydration. It can finally be noted that the larger sizes of the needles with respect to the Vicat test allows for the study of mortars.

2.3. Proctometer

The proctor is a needle mounted on a spring which gives a digital display of the force applied while the needle is manually pushed into the sample. The needle has a load bearing surface as the penetrometer (see Fig. 1). The speed at which this needle is driven in depends on the operator and the material stiffness at the time the measurement is performed. Jolin et al. [5] in the case of a straight needle and Armelin and Banthia [6] in the case of needles with tips larger than a supporting rods have shown that the evolution of stress with the penetration depth is constant after a certain penetration depth (15 mm in the case of a needle of diameter 9 mm). This means that rod above the tip does not play any role and that the measurement is mainly linked to the penetration of the tip itself.

2.4. Hilti needle gun

The Hilti needle test consists in shooting a nail into a material and measuring the penetration depth [7]. From a rheological point of view, one may consider that, when the test starts, the nail has received a given kinetic energy from the nail gun. Therefore, the nail should stop once that energy has been dissipated through the deformation of the tested material.

3. Experimental and numerical work

3.1. Experimental work

3.1.1. Materials

One single ordinary Portland cement (OPC) is used in this paper. This is because our aim is to demonstrate a basic physical or mechanical behaviour which is expected to be independent of the specific nature of the hydrating cement. Cement pastes are prepared by adding water into a Hobart mixer already containing the cement and mixing for 2 min. No admixture is included and the water to cement ratio W/C was 0.3.

3.1.2. Penetration tests

The paste is transferred into the measuring cell of a penetrometer and the needle is driven into the sample until the tip is fully submerged. At that point the measurement is initiated, causing the sample holder to rise at 1 μm/min, while the force on the needle is recorded. Several tip geometries (hemispherical tip, hemispherical tip and connected cylinder, conical tip and connected cylinder) are used. Experiments are conducted in parallel to eliminate any possible variations in cement paste properties. Some additional measurements are performed with two Vicat needles of different diameters.

3.1.3. Ultrasound propagation tests

In addition, some material is introduced into a specially built ultrasound spectrometer operating in echo mode with a shear transducer. The temporal evolution of a pulse ultrasonic attenuation at a plexiglass/cement interface is followed. Usual treatments of acoustic impedance are used to determine the shear modulus over time [8–10]. At the plexiglass/cement interface, one portion of the wave is reflected while the other is transmitted. A part of the wave is

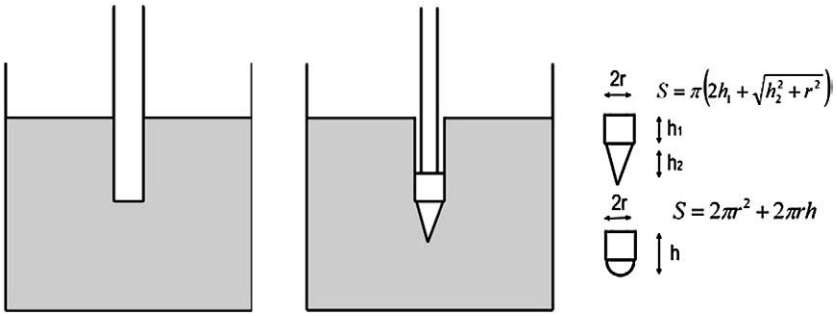

Fig. 1. Schematic illustration of the difference between Vicat needle and penetrometer tests. The Vicat needle is used in different locations and the load bearing surface decreases as the material stiffens (left). The penetrometer drives into the sample a needle of which the load bearing surface is constant over time (center). The expressions for those load bearing surfaces are given above for two needle geometries (right).

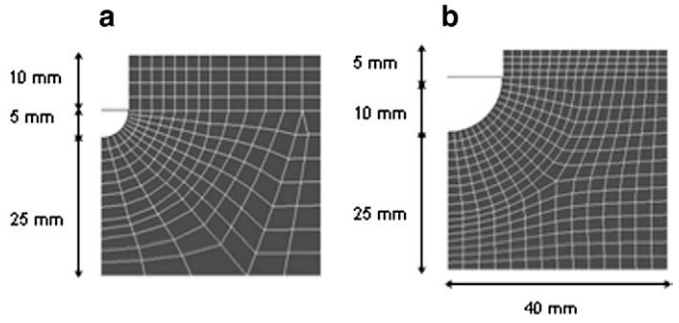

Fig. 2. Representation of the different tips used in the simulations and the associated mesh of the cementitious material. Cases a) and b) are for the hemisphere only.

reflected at the cement/plexiglass interface and goes back to the transducer. The pulse magnitude coming from the first interface reflection is linked to the acoustic impedances of the two mediums. The reflection coefficient *r*, which is the ratio of the amplitude of the reflected wave to the incident wave, is linked to the acoustic impedances of the two mediums:

$$r = \frac{A_r}{A_i} = \frac{Z_2 - Z_1}{Z_2 + Z_1} \tag{1}$$

The mechanical properties of the sample can be established with the knowledge of the acoustic impedance of the Plexiglas and the measure of *r*. In the case of reactive materials as cementitious materials, the signal evolves with time and ultrasound therefore provides a continuous, non destructive measure of mechanical properties.

3.2. Numerical work

3.2.1. Elasto plastic solid simulations

Finite element simulations of a penetrometer tip embedded in a large cylindrical body are carried out with the FEM Code Abaqus/Standard 6.6.1 [21] (see Fig. 2) under the following assumptions.

1. The penetrating tool was considered as perfectly rigid.
2. The tested material was defined either as purely elastic or ideally elasto-plastic. The most widely used elastoplastic theory is based on the following concepts:
   - The additive strain decomposition:

$$\varepsilon = \varepsilon^e + \varepsilon^p \tag{2}$$

   ε is the total strain, ε^e is the elastic strain (recoverable) and ε^p is the plastic strain
   - The elastic constitutive equation:

$$d\sigma = D : d\varepsilon^e \tag{3}$$

   σ denotes the Cauchy stress and D the fourth order elastic constitutive tensor
   - The definition of the elastic domain with the help of the yield function:

$$f(\sigma, \overline{\sigma}) \leq 0 \tag{4}$$

   $\overline{\sigma}$ is the yielding stress. It does not depend on the equivalent plastic strain $\bar{\varepsilon}^p$ in our specific case since no hardening is assumed.
   - The flow rule that governs the evolution of the plastic flow and defines its direction. The normality assumption, is generally used, i.e. the flow is assumed to be normal to the flow potential.

$$d\varepsilon^p = d\lambda \frac{\partial g}{\partial \sigma} \tag{5}$$

   g is he flow potential and $d\lambda$ is called the plastic multiplier. In our specific case the yielding function f is chosen as the flow potential ($g=f$) and the flow is said "associated".
   In the present study, the Prandt–Reuss [22] plasticity model has been used. This is an associated plasticity model that uses the von Mises yielding function:

$$f(\sigma, \overline{\sigma}) = q - \overline{\sigma} \tag{6}$$

   $q = \sqrt{\frac{3}{2}\sigma' : \sigma'}$ is the equivalent von Mises stress and σ' is the stress deviator.
   An important particularity is that the von Mises Yield function does not depend on the hydrostatic stress state in the material.
3. The contact surface between the tip and the cementitious material was considered either frictionless or displaying a friction coefficient of 0.13 (range of values used for metals, a probably reasonable upper bound).
   The friction model provided in Abaqus for this analysis was a classical isotropic Coulomb friction Model. The model assumes that no relative motion occurs if the equivalent frictional stress $\tau_{eq} = \sqrt{\tau_1^2 + \tau_2^2}$ is less than the critical stress, proportional to the contact pressure p in the form $\tau_{crit} = \mu p$ where μ is the friction coefficient.
4. Considering the sample geometry, an axisymetric mesh has been used for the simulation (Fig. 2) for simplicity and computational efficiency.

3.2.2. Visco-plastic fluid simulations

A 3D Bingham model is used to describe the tested fluid behaviour [11,12]. Moreover, in order to avoid the undetermination of the strain state in the zones where the yield criterion is not fulfilled, the material is assumed to behave as an incompressible elastic solid up to the yield stress, beyond which it behaves as a Bingham fluid. The computational fluid mechanics code Flow3D® [10,13] is chosen to solve the fluid mechanics equation (see Fig. 3). The invariant generalization of a Bingham fluid uses here is the one proposed by Oldroyd [14] based on a three dimensional von Mises yield criterion:

$$\boldsymbol{\Sigma}^{(d)} = \left[\tau_0 / \left|\left(\frac{1}{2}\mathbf{d} : \mathbf{d}\right)^{1/2}\right| + \mu_p\right]\mathbf{d}, \frac{1}{2}\boldsymbol{\Sigma}^{(d)} : \boldsymbol{\Sigma}^{(d)} \geq \tau_0^2, \tag{7}$$

where Σ and d are respectively the stress and strain rate tensors, τ_0 is the yield stress and μ_p the plastic viscosity. When the flow is

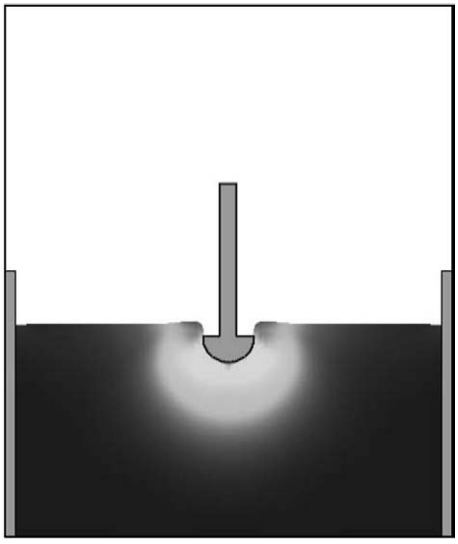

Fig. 3. Example of fluid simulations in the case of a hemispherical tip. The grey level indicates the stress level in the material. Dark zones are not sheared.

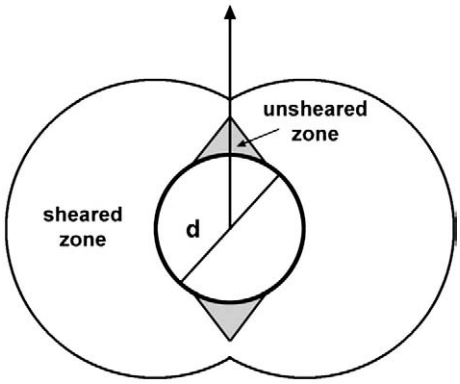

Fig. 4. Sheared and unsheared zones around a sphere moving in a yield stress fluid. The arrow represents the velocity vector.

dominated by shear stress and shear rate, the previous relation simplifies to the famous Bingham scalar model:

$$\tau = \tau_0 + \mu_p \dot{\gamma} \ , \tau \geq \tau_0 \tag{8}$$

4. Analysis of the penetrometer tests

4.1. Theoretical frame

From a rheological point of view, yield stress is the only feature of the material, which can stop a needle penetration. Indeed, as the needle is penetrating the sample, the surface supporting the applied load increases. As a consequence, the stress applied on the tested material decreases. As long as the weight of the needle or the applied force creates in the sample a stress higher than the yield stress, the needle keeps on penetrating the sample until the generated stress becomes lower than the yield stress and flow stops [15]. Of course, in the case of penetrometer test, as the penetration speed is imposed, flow cannot be stopped by yield stress but yield stress, as shown below, will be the main contribution to the force needed to maintain this penetration speed.

Focussing at this stage on penetrometer tests, it is interesting to note that these tests involve very low velocities and can thus be considered as quasi static flows. Therefore in first approximation the stress should be of the order of the yield stress. Indeed, there is a flow so the deformations are too high to consider that the material stays in the elastic regime. The stress is therefore higher than the yield stress. However, because the flow is so slow, the contribution of plastic viscosity is very low, meaning that the stress should stay very close to the yield stress.

In order to deduce the scale of the associated force knowing the order of magnitude of the stress, a surface is needed. The first option is to consider that this surface is the external surface of the tool and that the stress is equal to the yield stress everywhere at the interface between the tool and the tested material. However, it can be reminded here that, in this type of flow, the interface between the sheared zone and the unsheared zone is most of the time not located at the moving object surface even at low speed [16,17]. Zones of unsheared fluid are cohabiting with zones of sheared fluid as shown in Fig. 4 in the case of a sphere moving in a yield stress fluid. It is thus not possible to estimate the force just by simply multiplying the yield stress by the external surface of the moving object.

An illustration of these aspects can come from the elasto-plastic simulation carried out in this work. It can be seen in Fig. 5 that yield stress or plasticity plays a strong role. The material does not stay in the elastic regime and the force reaches a fixed value after a given penetration depth. Moreover, the friction coefficient does not play a role on this force. This confirms the fact that the boundary between sheared and unsheared zones is not located at the interface between the tool and the sample, which only plays a minor role in the flow.

Let us now go further and consider a penetrometer with no precisely defined shape. Here a yield stress fluid initially at rest is considered. As described in Section 3.2.2 a three dimensional yielding criterion taking into account the three dimensional stress field is also considered. The von Mises criterion provides a straightforward tensorial expression for describing the solid liquid transition:

$$\begin{aligned} &\sqrt{-T_{II}} < \tau_0 \Leftrightarrow \mathbf{d} = 0 \\ &\sqrt{-T_{II}} > \tau_0 \Leftrightarrow \boldsymbol{\Sigma}^{(d)} = \tau_0 \frac{\mathbf{d}}{\sqrt{-D_{II}}} + f(D_{II})\mathbf{d} \end{aligned} \tag{9}$$

where T_{II} is the second invariant of the deviatoric stress tensor $\mathbf{T}$; D_{II} is the second invariant of the deformation rate tensor and f is an increasing function.

A compact penetrating object of external surface S moving at steady velocity V is also considered. This object is thus submitted to a drag force $\mathbf{F}_D$ which corresponds to the force resisting motion due to the apparent viscosity of the fluid. Let us apply the momentum balance to the fluid volume situated between S and S^*, the external surface of a large volume including the object. In the absence of inertia effects:

$$-\mathbf{F}_D + \int_{S^*} \mathbf{T}.\mathbf{n} ds = 0 \tag{10}$$

The validity of this relation for any surface size and shape S^* implies that, in any direction, the local stress tensor tends towards zero as the distance from the object tends towards infinity. It results that, in any direction, beyond some critical distance, the yielding criterion is not satisfied, so that the fluid should remain rigid despite object motion. The set of the critical positions beyond which the yielding criterion is not fulfilled at a given time forms a surface S_c surrounding the object so that:

$$\mathbf{F}_D = \int_{S_c} \mathbf{T}.\mathbf{n} ds \tag{11}$$

On approach of S_c, the amplitude of the strain rate tensor tends towards zero, which implies, considering the yielding criterion, that the deviatoric stress tensor becomes proportional to the yield stress τ_0. It is therefore possible to conclude that the drag force is proportional to yield stress.

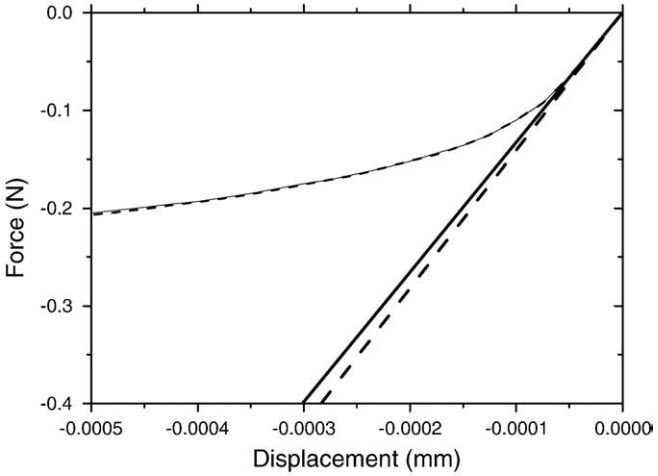

Fig. 5. Force displacement relation for a penetrometer tip with a hemisphere (radius of 5 mm) and connected cylinder (10 mm high). Data shows the force on the needle as a function of the displacement. The continuous lines are the frictionless case and the discontinuous ones those with a friction coefficient of 0.13. The straight lines are the elastic case, while the curved ones show the ideal elasto-plastic situation.

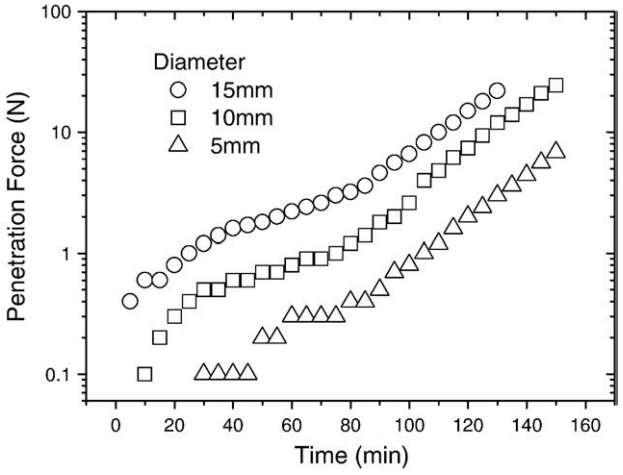

Fig. 6. Penetration force measured with three hemispherical tips of different diameters.

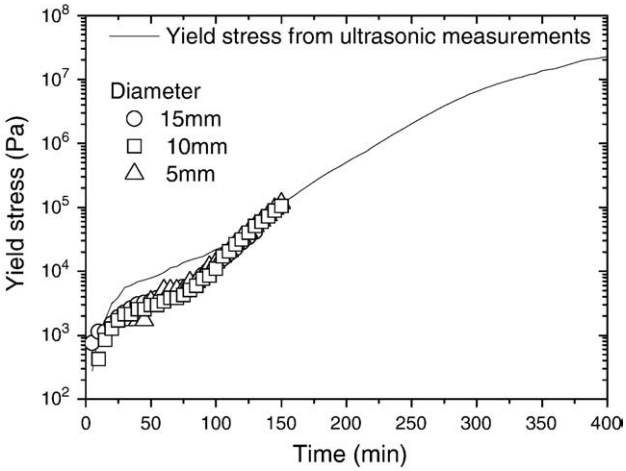

Fig. 7. Yield stress extrapolated from ultrasound shear modulus and penetrometer force measured with hemispherical tips of various diameters (see text).

4.2. Simple approach of the hemispherical tip case

In this particular case, an important aspect is that the needle tip is wider than the rod on which it is mounted. Consequently, samples with a yield stress above a minimum value (not defined here) do not close up the gap above the tip and the surface S through which the needle transmits stress to the sample is constant during the experiment as long as steady state has been reached.

It is assumed that Stokes law, although derived for a sphere in a Newtonian fluid, can be applied to the hemispherical tip. Half of the drag force needed for a complete sphere therefore writes:

$$F = 3\pi\eta RV \tag{12}$$

where η is the viscosity of the tested material, R is the hemispherical tip radius (see. Fig. 1) and V its imposed velocity.

If the material is assumed to follow a Bingham type behavior then:

$$\eta = \tau_0 / \dot{\gamma} + \mu_p \tag{13}$$

Substitution into Eq. (12) gives:

$$F = 3\pi R\left(\frac{\tau_0}{\dot{\gamma}} + \mu_p\right) V \tag{14}$$

For quasi-static flows, one does not have to worry about the plastic viscosity μ_p but only about the term $\tau_0/\dot{\gamma}$. Furthermore, for a sphere, it has been shown that the velocity gradient is well approximated by [14,11]

$$\dot{\gamma} \cong kV / R \tag{15}$$

where k is a constant close to unity. Substitution into Eq. (14) gives for quasi static flows:

$$F = 3\pi R^2 \tau_0. \tag{16}$$

Let us compare this relation with our experimental results. Forces measured with a penetrometer having needles in the shape of hemispheres with diameters 5, 10 and 15 mm are shown in Fig. 6 along with the shear modulus measured by ultrasound. It turns out that, as predicted by Eq. (16), the forces obtained with these needles superpose extremely well when they are divided by $3\pi R^2$ as represented in Figs. 6 and 7.

It also turns out that the shear modulus measured by ultrasound scales very well at long times with the yield stresses deduced from the needles penetration. This points to the fact that the force measured by the penetrometer is related to shear yield stress, which is consistent with [18,19]. The fact that the critical strain in cementitious materials is more or less constant during hydration [20], means that the force measured by penetrometers should generally scale with shear modulus although it is really a yield stress measurement through $\tau_0 = G\gamma_c$. The value of the critical shear deformation γ_c needed to rescale all results is here of the order of 0.005, which is a consistent value for concentrated colloidal systems [20]. At short times, it can be assumed that the biphasic nature of the suspension prevents the ultrasound technique from giving a proper measurement of the elastic shear modulus of the homogeneous material.

This scaling with the power 2 of the radius is also confirmed by our fluid dynamics simulations as represented in Fig. 8 which also shows an excellent agreement with the simple analytical solution proposed here. Moreover, as shown in Fig. 9, the penetration force is proportional to the yield stress of the material and does not depend, for the very low penetration velocities studied here, on the plastic viscosity. This confirms the quasi static nature of the flow.

4.3. Simple approach of the hemispherical tip and connected cylinder

The simplest way to take into account the connected cylinder is to add the contribution of the cylindrical part of the tool to the penetration force. Contrary to the case of a sphere moving in a yield stress fluid, the case of a cylinder moving along its axis is more simple. At flow initiation, the shear stress at the surface of the cylinder reaches the value of the

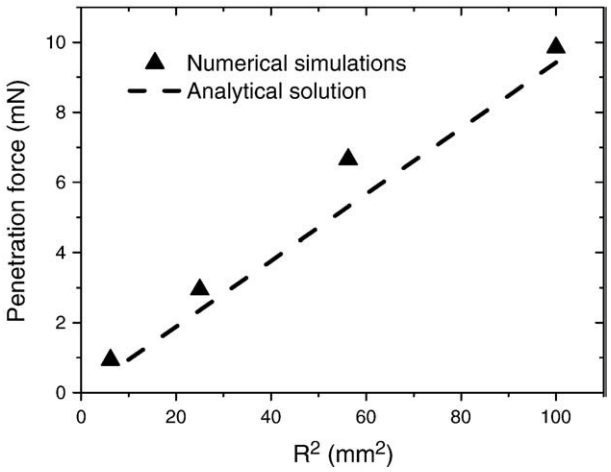

Fig. 8. Penetration force as a function of the power 2 of the radius in the case of a hemispherical tip. Yield stress 10 Pa. Radius of the container is 40 mm.

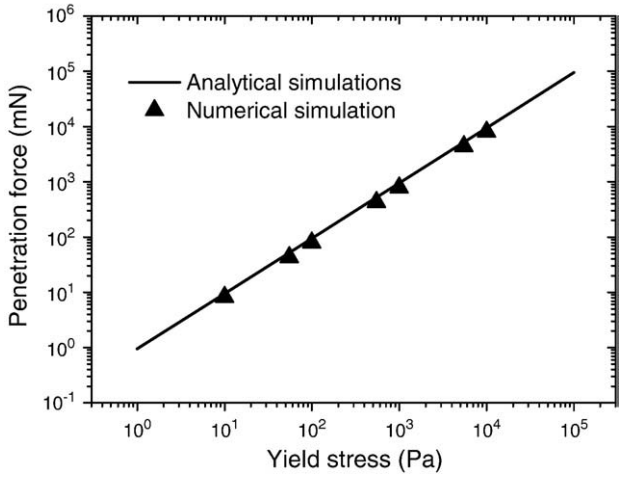

Fig. 9. Penetration force at a given penetration depth as a function of the material yield stress in the case of a hemispherical tip and connected cylinder. Calculus are carried out with plastic viscosities varying from 0.1 to 100 Pa s without noticing any influence of this parameter. Radius 10 mm and penetration speed 1 μm/s.

yield stress [14]. It is thus in theory sufficient to add the contribution of this additional surface although it has to be kept in mind that there must exist a transition zone between the hemispherical part and the cylinder in which the boundary between sheared and unsheared zones in the material reaches the tool. Eq. (16) becomes:

$$F = \left(3\pi R^2 + 2\pi Rh\right)\tau_0 \tag{17}$$

where h is the immersed depth of the cylinder.

As an extension to the previous tests, needles with a hemispherical end mounted on cylinders of same diameter but different lengths were used. Measured forces for diameters of 5 and 15 mm with heights of 0, 2, 10 and 15 mm are shown in Fig. 10. The obtained data, of course, do not superpose well. A better superposition is however obtained if one normalizes by the equivalent surface $3\pi R^2 + 2\pi Rh$ in Eq. (17) as showed in Fig. 11. In this way, one uses here units of surface, an approach that has also successfully been used in analyzing ball indentation penetrometer results [20]. However, the data series with the largest diameter and height remain outliers. This result is reproducible and may be the result of the needle size no more negligible compared to the cell size.

4.4. Simple approach of the conical tip and connected cylinder

Although there is no analytical solution in the case of a cone moving in a yield stress fluid, it seems rather logical to assume that, according to the shape of the object, the boundary between sheared and unsheared zones at initiation of flow is located at the surface of the object itself. The penetration force should then write:

$$F = \left(\pi R\sqrt{R^2 + h_2^2} + 2\pi Rh\right)\tau_0 \tag{18}$$

In a series of experiments with conical tips, the yield stress of the tested material is calculated by dividing the measured force by the surface $\pi R\sqrt{R^2 + h_2^2} + 2\pi Rh$ where h and h_2 are respectively the heights of the cylindrical and conical section (Cf. Fig. 1). The obtained results are in very good agreement with the other results from other tools as shown in Fig. 11.

4.5. Simple approach of the Vicat needle

The diameters of Vicat needles are small compared to their length. It is therefore possible to neglect the end effect of the tip compared to the length effect of the needle. This means that the contribution of the cylindrical part of the needle will dominate the contribution of the tip of the needle whatever its shape. This will of course not hold at the end of the test when the penetration depth is of the same order as the diameter of the needle. However, through the test, it is possible to write the penetration force under the following form:

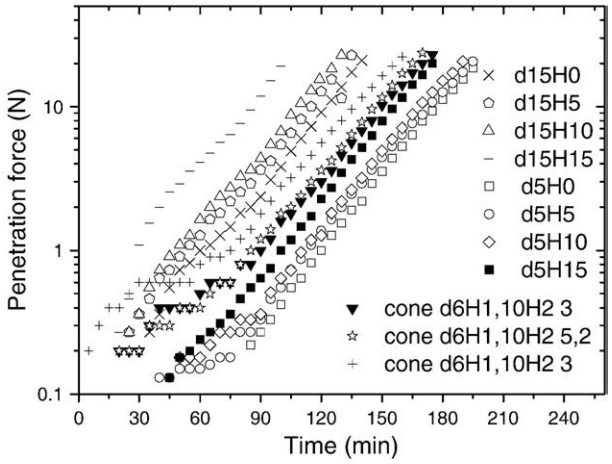

Fig. 10. Penetrometer force measurements with different tips. The first number in the legend is the diameter in mm of the hemispherical tip and the second number is the height of the cylindrical section of same diameter placed above.

$$F = 2\pi Rh\tau_0 \tag{19}$$

The penetration force is equal to the load of the needle (300 g) and the yield stress can therefore be deduced from the penetration depth. It could of course be noticed that the assumption of a quasi static flow does not seem to hold *a priori* for a falling loaded needle. However, it seems, according to our experimental results, that what matters is the conditions under which the Vicat needle stops. As the needle is stopping, the flow may again be considered as slow and the contribution of the plastic viscosity neglected.

The extrapolated yield stresses are plotted in Fig. 11 and are once again very well correlated to the other type of measurements. It may be useful to note here that, according to Eq. (19), the Vicat initial time of setting for cement pastes (ASTM C191-04b), which corresponds to a penetration depth of 25 mm of a needle of 1 mm diameter loaded with 300 g, can be associated to a yield stress of order 40 kPa. Similarly, the Vicat initial time of setting for mortars (ASTM C807-05), which corresponds to a penetration depth of 10 mm of a needle of 2 mm diameter loaded with 400 g, can be associated to a yield stress of order 50 kPa.

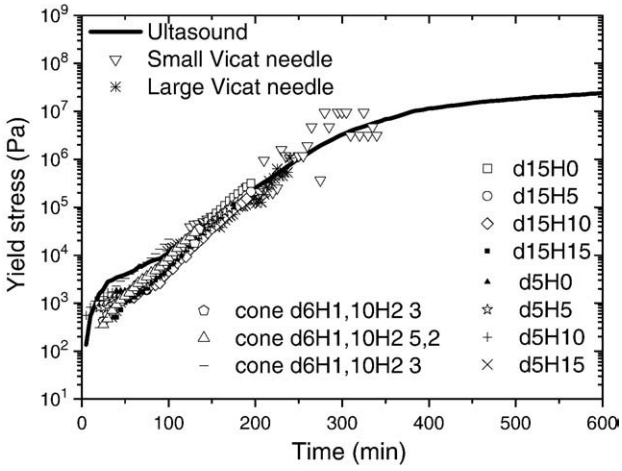

Fig. 11. Yield stress extrapolated from penetrometer force measurements with different tips, ultrasound measurements and Vicat needles.

4.6. Particular case of the shot Hilti needle

In the Hilti needle test, a needle is shot into a cementitious material and the penetration depth is taken as indicative of strength. Data are generally analyzed in terms of the Bracher Table [7]. This relates compressive strength to penetration depth through the following empirical exponential function (continuous line in Fig. 12).

$$C_S = C_{S_0} + C_{S_1}\exp\left(-\frac{P}{P_0}\right) \tag{20}$$

where $C_{S_0} = 5.10^3$ Pa, $C_{S_1} = 6.10^7$ Pa and $P_0 = 25.7$ mm.

For this type of test, it seems natural to consider that the needle is given a certain (constant) kinetic energy E_0 through the shooting and that it stops once this energy has been fully dissipated by the friction with the material. In this case, the role of plastic viscosity is most probably not negligible. However, as a first approximation, it is neglected and the dissipated energy is written as:

$$E_0 = \int_0^H F\,dH \tag{21}$$

Considering the shape of the needle and by neglecting the contribution of the needle, one can use here Eq. (19) and write:

$$E_0 = 2\pi R\tau_0 \int_0^H h dH = \pi R H^2 \tau_0 \tag{22}$$

It can be assumed that compressive strength C_S measured using ASTM C39/C39M-04a scales with the shear yield stress as they should both scale on the same critical deformation at failure. It becomes therefore possible to write that compressive strength scales with the inverse of the power two of the penetration depth.

$$C_S = A / H^2 \tag{23}$$

where A is a fitted constant, which depends on the kinetic energy given to the needle, the radius of the needle and on the relation between yield stress and compressive strength. The fitted value of A is of the order of 18,000 MPa mm^2. It seems that the relation proposed here is able to predict Bracher's data with only one fitted parameter instead of the three fitted parameters in Eq. (20).

5. Conclusions

Penetration tests are widely used to follow cementitious materials during setting. Despite limited quantification of the physical properties probed by these tests practical experience shows their usefulness. In this paper, it is inferred that these tests share a number of similarities and that a detailed investigation of one of them should shed light onto the others.

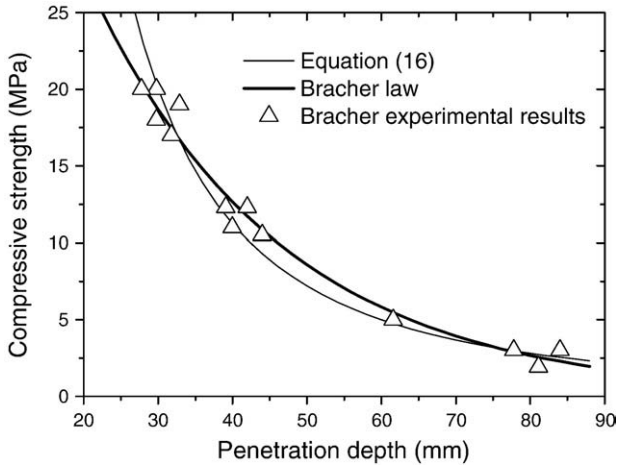

Fig. 12. Hilti needle data from Bracher. The bold line corresponds to Eq. (20), while the thin line corresponds to Eq. (23).

Table 2
Relations between test measurement and yield stress or compressive strength.

Test	Measurement type	Correlation with yield stress or compressive strength
Vicat with a needle of radius R	Measurement of penetration depth h in mm for an imposed load of 300 g.	$\tau_0 = \frac{3}{2\pi Rh}$
Hemispherical penetrometer of radius R	Measurement of a force F to maintain a given speed.	$\tau_0 = \frac{F}{3\pi R^2}$
Hemispherical penetrometer of radius R and connected cylinder of height h	Measurement of a force F to maintain a given speed.	$\tau_0 = \frac{F}{3\pi R^2 + 2\pi Rh}$
Conical penetrometer of radius R and cone height of $h2$ and connected cylinder of height h	Measurement of a force F to maintain a given speed.	$\tau_0 = \frac{F}{\pi R\sqrt{R^2 + h_2^2} + 2\pi Rh}$
Hilti needle	Measurement of penetration depth h in mm.	$C_S = \frac{18{,}000}{h^2}$

The case of penetrometer has been examined in detail with various needles, using experiments, finite element and fluid dynamics simulations. All results combine well to demonstrate that the measured force scales with the yield stress of the tested material. However, since the critical shear strain in cementitious materials is more or less constant, this force also scales directly with shear modulus and thus with results from ultrasonic techniques. Owing to the practical importance of yield stress, it is not surprising that these apparently empirical tools are widely used.

From this analysis, an analytical correlation has been derived (or semi-empirical in the case of the Hilti needle) which allows for the calculation of the yield stress of the material from the experimental measurement (or compressive strength in the case of the Hilti needle). These relations are gathered in Table 2. They constitute, in our opinion, a very useful library of correlations allowing for the comparisons of different test results and for the calculation of physical parameters from simple tests data.

Acknowledgements

The authors are thankful to Prof. Milan Jirasek (Czech Technical Univ., Prague) for critical feedback on a previous version of this manuscript. The authors also wish to thank the French competitiveness cluster Advancity and the Region Île de France for their financial help.

References

[1] D. Lootens, N. Roussel, R.J. Flatt, Rheology of penetration tests II: link to shear modulus. 12th ICCC, Montreal, Canada, July 8–13 2007.
[2] P. Jousset, D. Lootens, N. Roussel, R.J. Flatt, Rheology of penetrations tests I: theory and finite element simulations, 12th ICCC, Montreal, Canada, July 8–13 2007.
[3] L. Nachbaur, Etude de l'influence d'electrolytes sur l'hydratation et la prise du silicate tricalcique, composant principal du ciment Portland. Caracterisation des interactions a l'origine de la prise. PhD thesis, University de Bourgogne, 1997.
[4] L. Struble, T.Y. Kim, H. Zhang, Setting of cement and concrete, Cement and Concrete Aggr 23 (2) (2001) 88–93.
[5] M. Jolin, D. Deaupré, S. Mindess, Tests to characterise properties of fresh dry-mix shotcrete, Cement and Concrete Research 29 (1999) 753–760.
[6] H.S. Armelin, N. Banthia, Mechanics of aggregate rebound in shotcrete—(part I), RILEM Materials and Structure 31 (1998) 91–98.
[7] Österreichische Vereinigung für Beton- und Bautechnik, Richtlinie Spritzbeton, f. Csöngei GmbH, 2004, Wien.
[8] E. Nonnet, N. Lequeux, P. Boch, Elastic properties of high alumina cement castables from room temperature to 1600 °C, Journal of the European Ceramic Society 19 (1999) 1575–1583.
[9] Y. Akkaya, T. Voigt, K. Subramaniam, S. Shah, Nondestructive measurement of concrete strength gain by an ultrasonic wave reflection method, Materials and Structures 36 (262) (2003) 507–514.
[10] Lootens, D. Ciment et suspensions concentrées modèles. Ecoulement, encombrement et floculation. PhD thesis, Paris VI, 2004.

[11] N. Roussel, M.R. Geiker, F. Dufour, L.N. Thrane, P. Szabo, Computational modeling of concrete flow: general overview, Cement and Concrete Research 37 (2007) 1298–1307.
[12] N. Roussel, Rheology of fresh concrete: from measurements to predictions of casting processes, RILEM Materials and Structures 40 (10) (2007) 1001–1012.
[13] N. Roussel, Correlation between yield stress and slump: comparison between numerical simulations and concrete rheometers results, Materials and Structures 39 (4) (2006) 501–509.
[14] J.G. Oldroyd, A rational formulation of the equations of plastic flow for a Bingham solid, Proceedings of the Cambridge Philosophical Society 43 (1947) 100–105.
[15] P. Coussot, Rheometry of Pastes, suspensions and granular materials: Applications in Industry, J Wiley & Sons, 2005, pp. 246–253, ch. 7.
[16] N. Roussel, A theoretical frame to study stability of fresh concrete, RILEM Materials and Structures 39 (1) (2006) 81–91.
[17] R. Hill, The mathematical theory of plasticity, (Oxford University Press), Oxford, 1950.
[18] W. Johnson, Engineering plasticity, 1985 ch. 14.
[19] L. Nachbaur, J.C. Mutin, A. Nonat, L. Choplin, Dynamic mode rheology of cement and tricalcium silicate pastes from mixing to setting, Cement and Concrete Research 31 (2001) 183–192.
[20] L. Chapoy, J. Aklonis, The design and calibration of a stress relaxation ball indentation penetrometer, Transactions of the Society of Rheology 13 (3) (1968) 445–455.
[21] ABAQUS-Version 6.6, Users Manual, ABAQUS, Inc., Rhode Island, USA, 2003.
[22] R. Hill, The Mathematical Theory of Plasticity, Oxford University Press, 1950.